

RESEARCH

Open Access



Neutrophil membrane-derived nanoparticle loading TLR7 agonists augments radiotherapy efficacy and boosts abscopal effect via regulating tumor microenvironment

Dehua Lu¹, Yanming Xu², Xiaodong Yang², Ying Li¹, Mengqing Li², Yuanyuan Zheng², Yuenan Wang¹, Weihu Wang³, Shubin Wang², Jing Gao^{2*} and Yajie Liu^{1*}

*Correspondence:
gaojing_pumc@163.com;
Anthea1966@163.com

¹ Department of Radiation Oncology, Shenzhen Key Laboratory of Gastrointestinal Cancer Translational Research, Cancer Institute, Peking University Shenzhen Hospital, Shenzhen Peking University-Hong Kong University of Science & Technology Medical Center, Shenzhen 518036, China

² Department of Oncology, Shenzhen Key Laboratory of Gastrointestinal Cancer Translational Research, Cancer Institute, Peking University Shenzhen Hospital, Shenzhen Peking University-Hong Kong University of Science & Technology Medical Center, Shenzhen 518036, China

³ Department of Radiation Oncology, Key Laboratory of Carcinogenesis and Translational Research (Ministry of Education/Beijing), Peking University Cancer Hospital and Institute, Beijing 100142, China

Abstract

Background: Increasing evidence indicates that radiotherapy (RT) has synergistic inhibitory efficiency with immunotherapy agents in multiple cancers and enhances abscopal effects by regulating the innate immune response, which was further investigated in this study. Neutrophils are recruited in radiated tumors. Therefore, neutrophil membrane-coated nanoparticles potentially deliver R837 (Toll-like receptor 7 agonist) to radiated tumors.

Methods: A novel nanoparticle R837@PLGA@Neu was prepared by initially assembling PLGA (poly (lactic-co-glycolic acid)) with R837 (TLR7 agonist) into R837@PLGA followed by coating with neutrophil membrane. Characterizations of R837@PLGA@Neu were performed. Tumor targeting efficiency was evaluated by in vivo fluorescent imaging of CT26-bearing mice. Treatments of R837@PLGA@Neu combined with RT were carried out in unilateral and bilateral CRC tumor-bearing mice, followed by validations of immune cells in tumors by flow cytometry.

Results: The characteristics of R837@PLGA@Neu were well identified, and it was confirmed to have high uptake ability and low cytotoxicity in colorectal cancer (CRC) cells in vitro, as well as its strong tumor-targeting efficiency in vivo in CRC tumor-bearing mice. The exciting findings were that R837@PLGA@Neu combined with RT exerted prominent tumor inhibition not only in radiated tumors, but also in distant tumors without RT, suggesting its enhancement of the efficacy and abscopal effect of RT. The possible underlying mechanisms were remodeling of the tumor microenvironment by triggering mature dendritic cells and CD8⁺ T cells.

Conclusion: In summary, our findings suggested that neutrophil membrane-derived nanoparticle R837@PLGA@Neu with high uptake ability and low cytotoxicity showed strong tumor-targeting efficiency, and combination with RT had a promising effect in CT26-bearing mice via immune cell regulation. Our results provide a probable combination strategy for CRC treatment.

Keywords: Radiotherapy, Abscopal effect, TLR7 agonist, Neutrophil membrane, Nanoparticle



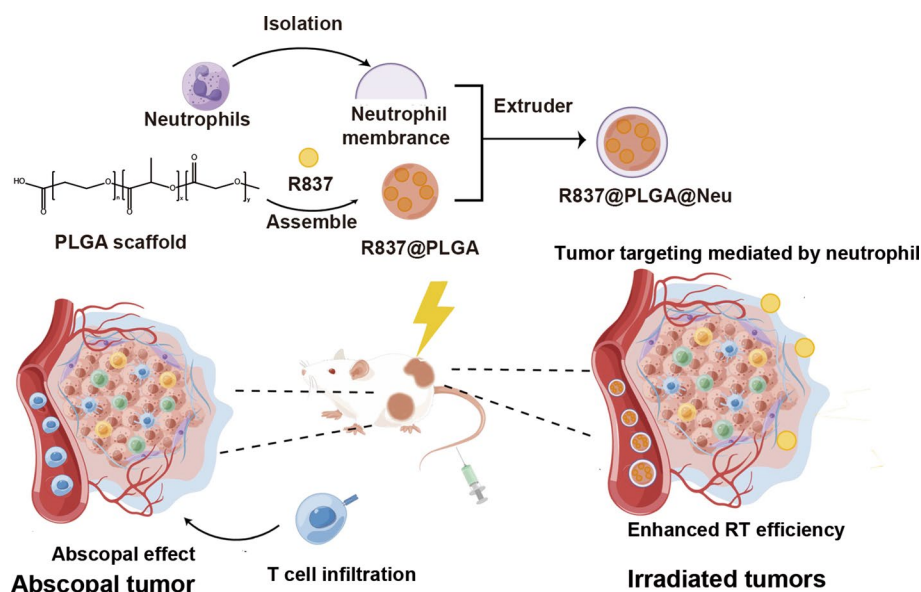
Introduction

In addition to chemotherapy and surgery, radiotherapy (RT) is one of the three treatment modalities in clinical oncology and is currently administered to over 50% of cancer patients (Miller et al. 2019). RT was confirmed to induce an “abscopal effect” (Reynders et al. 2015), which referred to the shrinkage of nonirradiated or metastatic lesions when RT was performed on the local lesion. Recently, with the wide application of immunotherapy represented by immune checkpoint inhibitors (ICIs) in cancer, RT was proven to promote antitumor immunity by regulating the immune system (Donlon et al. 2021). Therefore, great concerns have focused on the combination of immunotherapy and RT in various types of solid tumors to achieve synergistic inhibition (Xu et al. 2022). Additionally, RT combined with immunotherapy could induce an increased frequency or intensity of the abscopal effect, which has attracted a variety of explorations in multiple cancers.

R837 (also called Aldara or imiquimod) is a toll-like receptor 7 (TLR7) agonist approved by the US Food and Drug Administration (FDA) and exhibits prominent antitumor and antiviral effects by activating the innate immune response (Miller et al. 1999). R837 cream has been approved for treatment against basal carcinoma (Panelli MC et al. 2007). Furthermore, R837 treatment enabled antitumor immunity after RT in cancer (Ito 2016). Theoretically, the innate immune agonist R837 showed great potential in enhancing RT efficiency and inducing abscopal effects (Walshaw et al. 2020). However, the low water solubility of R837 impedes its systematic delivery and limits its clinical transformation, which needs to be further resolved.

Nanoparticles have been confirmed to be a promising agent to achieve systematic delivery of low water solubility drugs with high targeting efficiency (Varshney et al. 2021). Tumor infiltration of R837 was increased by encapsulation with polymeric nanoparticles fabricated with poly (lactic-co-glycolic acid) (PLGA), a biocompatible polymer approved for clinical use by the FDA (Chen et al. 2019). Polyethylene glycol (PEG)-grafted PLGA showed higher biocompatibility, and R837 loaded by PEG-modified PLGA enhanced RT efficiency in murine tumor models (Zhao et al. 2021). However, PLGA polymers passively accumulate in tumors by the enhanced permeability and retention (EPR) effect (Meng et al. 2018), resulting in limited tumor-targeting efficiency. Therefore, it is urgent to design a novel nanoparticle with high biocompatibility and sufficient drug delivery to tumors.

Surface modification of nanoparticles mimicking the cell membrane creates new opportunities for developing nanoparticles in biomedical applications (Gong and Winnik 2012). After the first report on red blood cell mimicking as a drug delivery system (Hu et al. 2011), more studies have explored cell mimicking into different types of cells to encapsulate multiple nanoparticles. Higher biocompatibility and prolonged retention time in vivo were featured in these reports (Cao et al. 2016). Cell membrane-coated nanoparticles have shown great potential in clinical translational research. Studies have shown that RT can induce the stimulated release of various cytokines and recruit immune cells (Barker et al. 2015). Shortly after RT, cytokines such as interleukin-8 (IL-8) are largely produced and mediate the accumulation of neutrophils in tumors to induce acute inflammation (Citrin et al. 2012; Takeshima et al. 2016). Ju C, et al. suggested the



Scheme 1 Illustration of synthetic procedures for R837@PLGA@Neu. After tail vein injection, R837@PLGA@Neu nanoparticles were targeted into tumor tissue after RT. Enhanced antitumor immunity was induced by the TLR7 agonist R837 in local tumors that received RT, and the systematic immune response mediated by activated T cells triggered an abscopal effect in distant tumors

possibility of drug delivery using neutrophils to improve treatment efficiency in gastric cancer after RT (Ju et al. 2019).

Herein, in this study, a novel nanoparticle R837@PLGA@Neu was prepared using neutrophil membrane and used to deliver R837 to tumors and boost the abscopal effect. This work can provide evidence for further study and clinical translation of cell-mimicking nanoparticles combined with RT.

Results

Characterization of R837@PLGA @Neu nanoparticle

Scheme 1 illustrates the overall process of neutrophil membrane-coated nanoparticles and a diagram of combination therapy in tumors. The preparation diagram of R837@PLGA@Neu is shown in Fig. 1A by the initial assembly of PLGA with R837 into R837@PLGA followed by coating with neutrophil membrane. After the synthesis of nanoparticles, the characteristics of R837@PLGA and R837@PLGA@Neu, including morphology, size distribution, zeta potential, and R837 release ability, were evaluated by TEM, DLS, and HPLC, respectively. The results indicated that R837@PLGA@Neu was successfully surrounded by a membrane (Fig. 1B) and had a larger diameter than R837@PLGA (250.2 ± 54.7 nm vs. 180.9 ± 41.9 nm; Fig. 1C), which was also confirmed by fluorescent dye-labeled nanoparticles (Additional file 1: Fig. S1). The zeta potentials of R837@PLGA and R837@PLGA@Neu were -15.67 ± 1.03 mV and -18.43 ± 1.90 mV (Fig. 1D), respectively, suggesting their good stability. Moreover, R837 was slowly released for over 96 h, with a cumulative release of 50% for R837@PLGA and 40% for R837@PLGA@Neu (Fig. 1E).

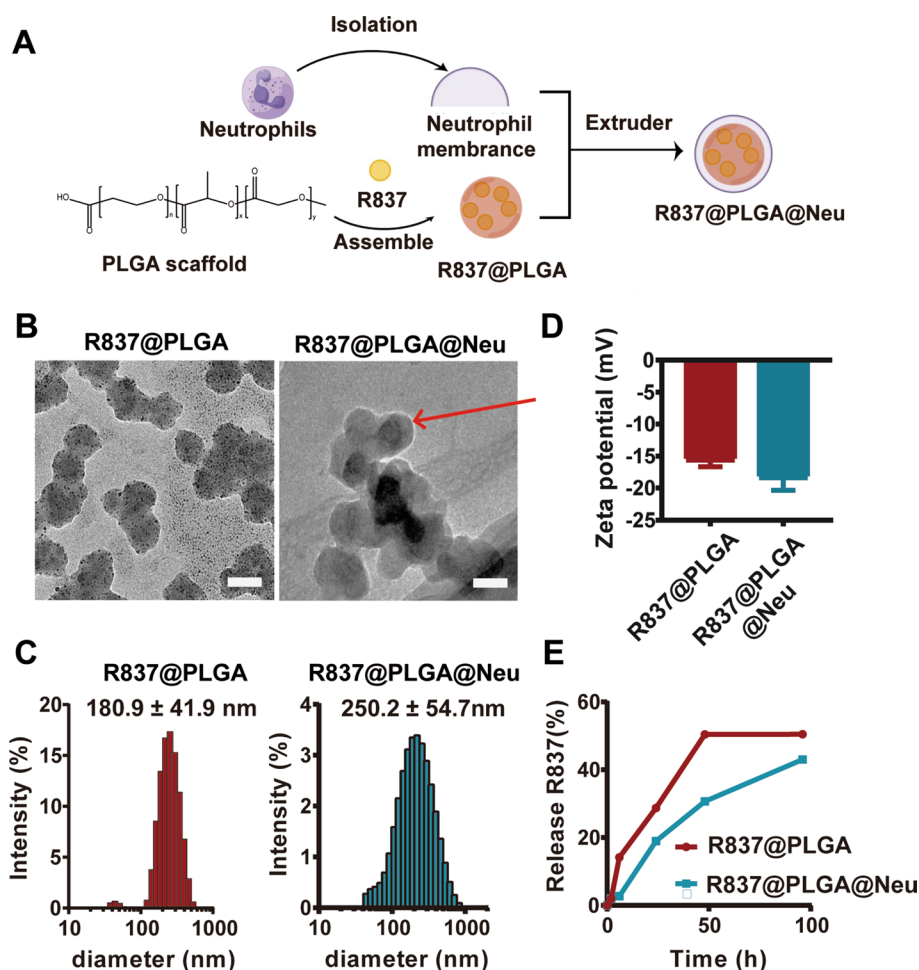


Fig. 1 Synthesis and characterization of R837@PLGA@Neu. **A** Schematic drawing of R837@PLGA@Neu synthesis. **B** Representative images of TEM screening of R837@PLGA and R837@PLGA@Neu (Scale bar: 50 nm). The red arrow indicates the membrane surrounding the nanoparticle. **C** Hydrodynamic diameters of R837@PLGA and R837@PLGA@Neu. **D** Surface zeta potentials of R837@PLGA and R837@PLGA@Neu ($n = 3$). **E** Drug release efficiency of R837@PLGA and R837@PLGA@Neu detected by HPLC. Data are presented as the mean \pm SD

R837@PLGA@Neu showed high uptake and low cytotoxicity in CRC cells in vitro

Colorectal cancer (CRC) cells were used in this study to explore the uptake, cytotoxicity, and efficiency of nanoparticles. Murine CT26 CRC cells were cultured in vitro in two-dimensional (2D) and three-dimensional (3D) patterns, cocultured with DyLight594-labeled nanoparticles for 24 h and observed under a fluorescence microscope (Fig. 2A, B). The uptake of nanoparticles by cells was high and indicated the following meaningful explorations. Therefore, CT26 cells were treated with R837@PLGA or R837@PLGA@Neu for 0, 24, 48, and 72 h, and cell viability was measured. We found that nanoparticles had no inhibitory effect on cells (Fig. 2C), which was further confirmed in other CRC cells treated with nanoparticles for 72 h (Fig. 2D), suggesting the low cytotoxicity of nanoparticles. Moreover, compared to the control, no obvious differences in cell apoptosis were found in CT26 cells treated with nanoparticles (Fig. 2E), representing low levels of early apoptosis (< 3%) and late apoptosis (< 1.5%).

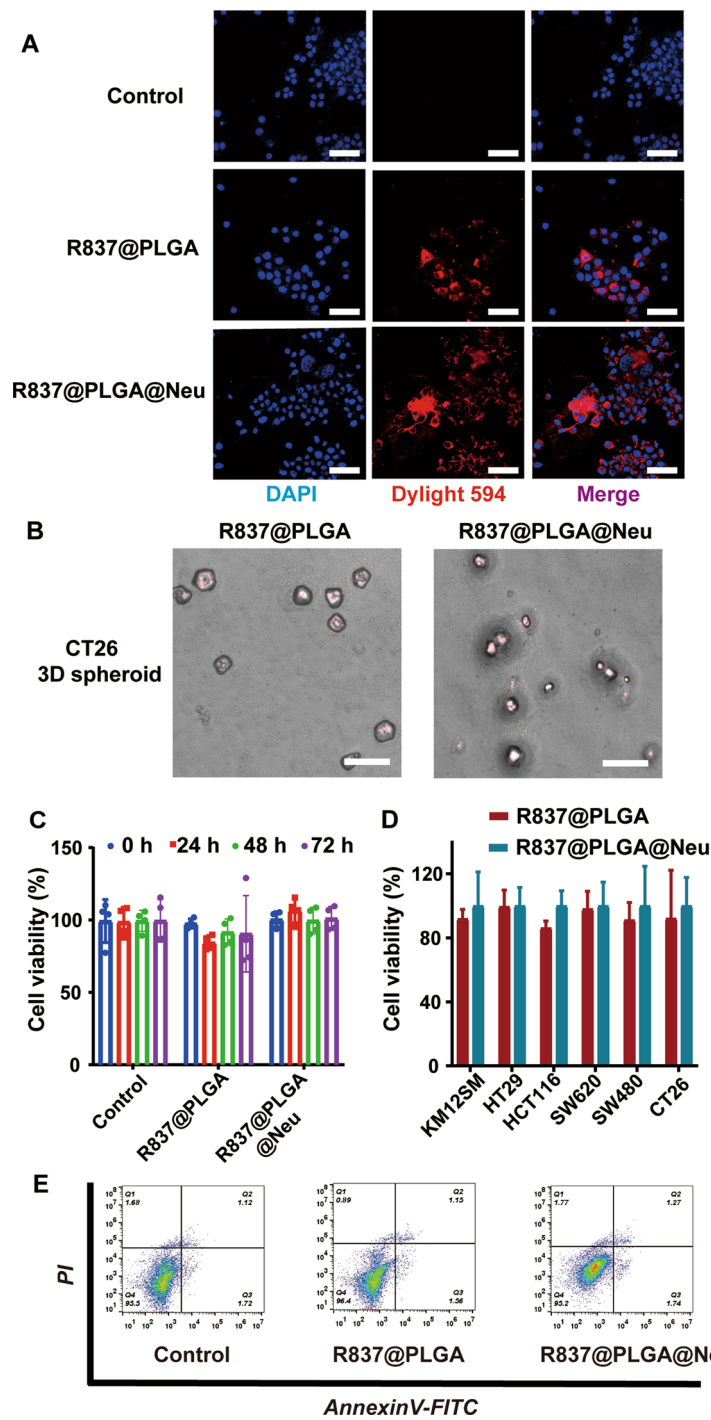


Fig. 2 In vitro cell uptake and cytotoxicity of R837@PLGA@Neu in CRC cell lines. **A** Confocal images of cell uptake of DyLight594 (red) labeled R837@PLGA or R837@PLGA@Neu in CT26 cells (scale bar: 50 nm). Blue represents DAPI staining of the cell nucleus. **B** Images of cell uptake of DyLight594 (red) labeled R837@PLGA or R837@PLGA@Neu in 3D spheroids of CT26 cells (scale bar: 100 μ m). **C** Cell viability of CT26 cells treated with R837@PLGA or R837@PLGA@Neu for 0, 24, 48, and 72 h. **D** Cell viability of CRC cells treated with R837@PLGA or R837@PLGA@Neu for 72 h. **E** Representative flow cytometric plots of cell apoptosis after treatment with R837@PLGA or R837@PLGA@Neu. All numerical data are presented as the mean \pm SD

High tumor uptake of R837@PLGA@Neu in vivo radiated CT26-bearing mice

Mice carrying unilateral subcutaneous tumor derived from CT26 cells were injected with DyLight649 labeled nanoparticles. The fluorescence signal in the tumor was detected after injection of nanoparticles for 4, 24 and 48 h with an uptake peak at 24 h (Fig. 3A), as well as the quantitative fluorescence signal (Fig. 3B). To explore the influence of RT on the tumor uptake of nanoparticles, a mouse bearing bilateral subcutaneous tumors derived from CT26 cells was established. RT was only performed on the tumor of the right flank followed by quick injection of DyLight649-labeled nanoparticles via the tail vein. From Fig. 3C, both radiated and nonradiated tumors had high uptake of nanoparticles with a stronger fluorescence signal of DyLight649-labeled R837@PLGA@Neu observed in radiated tumors compared to nonradiated tumors. Moreover, compared to R837@PLGA, RT enhanced the uptake of R837@PLGA@Neu, indicating the higher targeting efficiency of nanoparticles coated with neutrophil membranes (Fig. 3D, E).

RT had synergistic inhibitory efficacy with R837@PLGA@Neu in vivo

Unilateral CT26 cell-derived tumor-bearing mice were treated as shown in Fig. 4A with RT three times and nanoparticle administration one time. Interestingly, either R837@

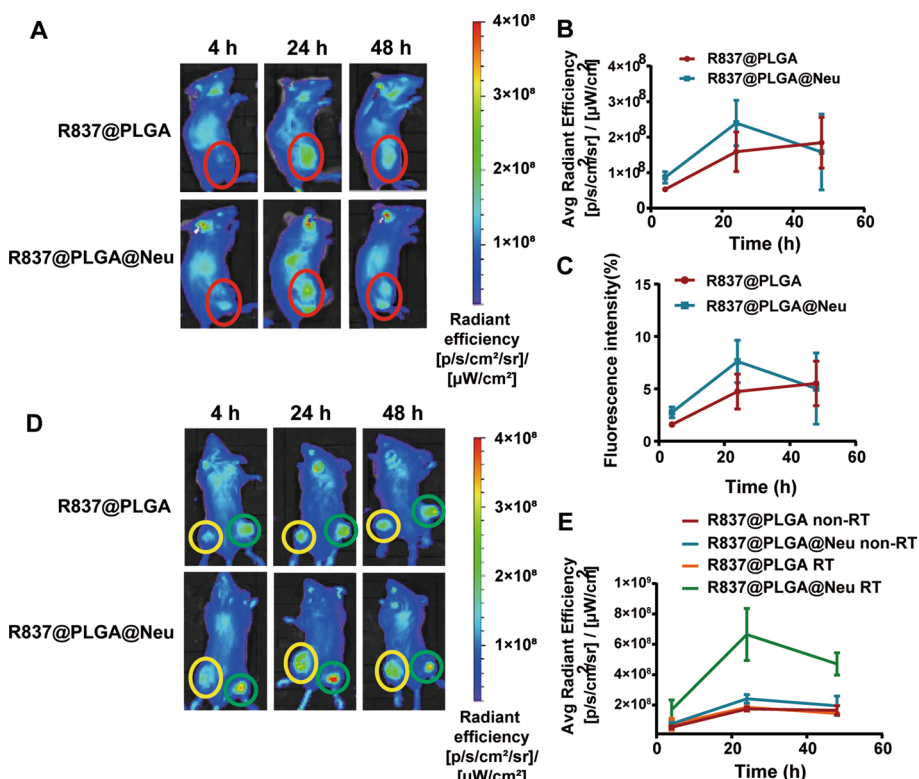


Fig. 3 Fluorescence images of CT26 tumor-bearing mice. **A** Fluorescence images taken at 4 h, 24 h, and 48 h after injection of DyLight649 labeled R837@PLGA or R837@PLGA@Neu. The red circle indicates xenografts in the mice. **B** The average radiant efficiency of fluorescence images in **A**. **C** The fluorescence intensity of fluorescence images in **A**. **D** Fluorescence images taken at 4 h, 24 h, and 48 h after injection of DyLight649 labeled R837@PLGA or R837@PLGA@Neu in bilateral tumor-bearing mice. The green circle indicates xenografts receiving RT, and the yellow circle indicates xenografts without RT. **E** The average radiant efficiency of fluorescence images in **D**. All numerical data are presented as the mean ± SD

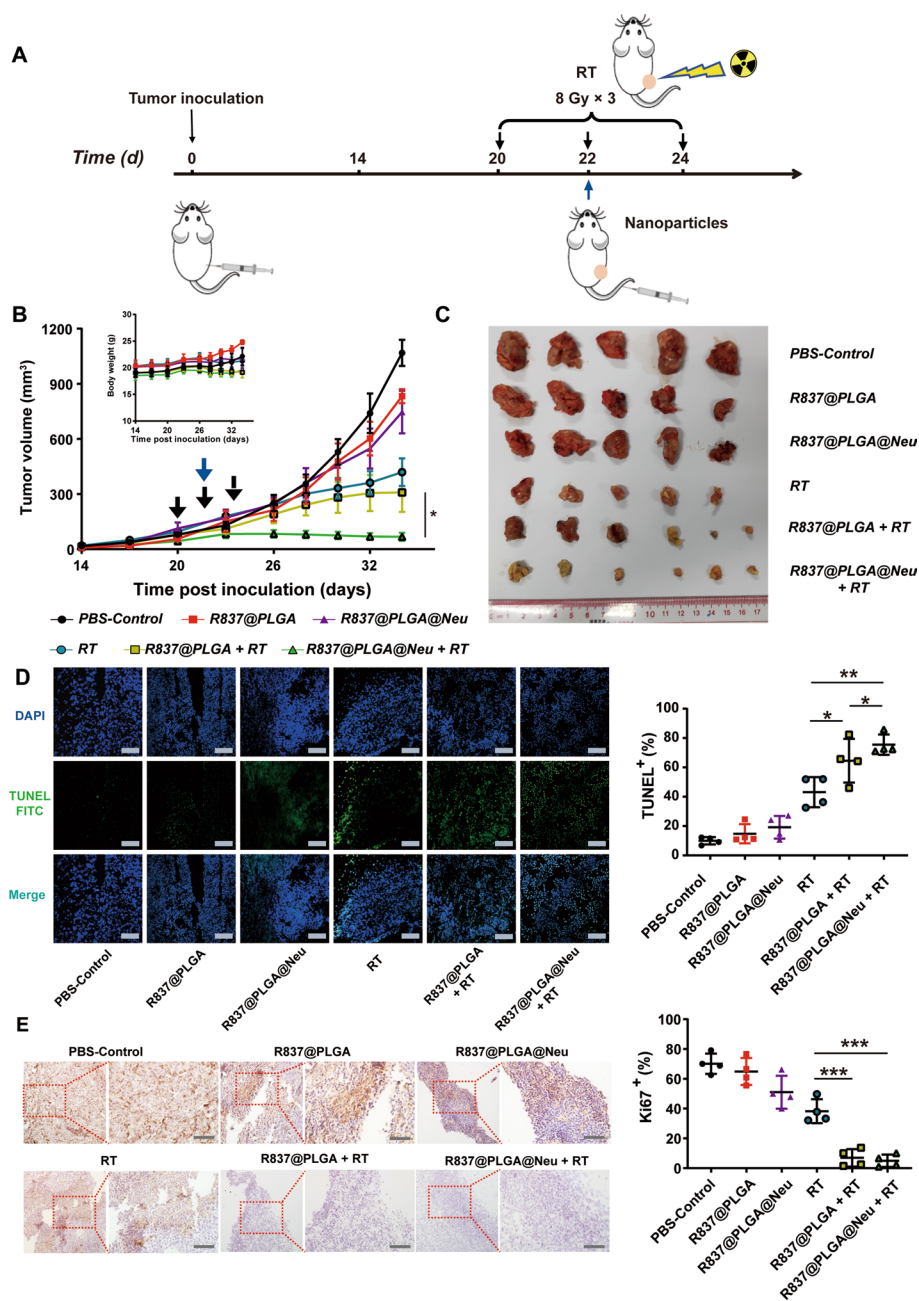


Fig. 4 The efficacy of RT combined with R837@PLGA or R837@PLGA@Neu in vivo. **A** Schematic illustration of combination therapy in vivo. **B** Tumor growth curves and body weights of mice in different groups. **C** Photographs of isolated tumors at the endpoint after the indicated treatments. **D** Representative figures of TUNEL staining and quantitative analysis of TUNEL-positive cells in tumor tissues after treatments (scale bar: 50 μ m). **E** Representative figures of IHC staining of Ki67 and proportions of Ki67-positive cells in tumor tissues after treatments (scale bar: 50 μ m). Numerical data are presented as the mean \pm SD. * P < 0.05; ** P < 0.01; *** P < 0.001

PLGA (TGI = 21.37%) or R837@PLGA@Neu (TGI = 35.95%) had very weak tumor suppression, and RT (TGI = 67.18%) or RT combined with R837@PLGA (TGI = 76.71%) exerted moderate inhibitory effects compared to the control (Fig. 4B, C and Additional file 1: Fig. S2). However, tumor inhibition was significantly enhanced in the RT

combined with R837@PLGA@Neu group, with a TGI of 97.61%. Moreover, nanoparticles alone or combined with RT had no obvious toxicity to mice, as indicated by undiscovered mouse weight loss, inflammation or cellular damage in critical organs (Fig. 4B and Additional file 1: Fig. S3). Further studies demonstrated that RT combined with nanoparticles could significantly induce cell apoptosis (Fig. 4D) and inhibit cell proliferation (Fig. 4E) in xenografts. This result indicated that our prepared nanoparticle R837@PLGA@Neu had potential clinical prospects with RT in CRC treatment with high efficacy and low toxicity.

RT synergized with R837@PLGA@Neu by triggering antitumor immune cells

Cell suspensions from xenografts treated with nanoparticles alone, RT alone or nanoparticles combined with RT were analyzed for the presence of immune cells by flow cytometry. CD45⁺ cells were gated to determine the CD4⁺ T cell and CD8⁺ T cell proportions (Additional file 1: Fig. S4A and Fig. 5A). For CD4⁺ T (CD45⁺CD4⁺) cells, no significant differences were found in each group of tumors (Fig. 5B); however, for CD8⁺

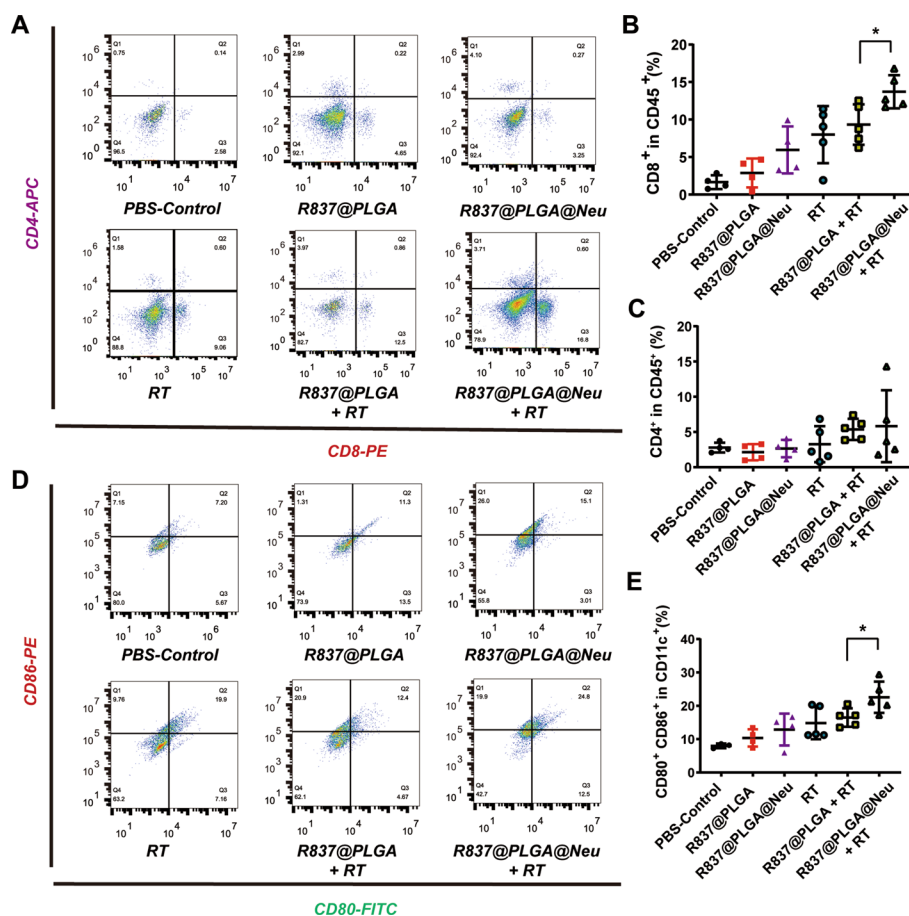


Fig. 5 Immune cell analysis of tumors after the indicated treatments. **A** Representative flow cytometric plots of CD4⁺ and CD8⁺ T cells in tumors after treatment. **B** Proportion of CD8⁺ T cells in CD45⁺ cells. **C** Proportion of CD4⁺ T cells in CD45⁺ cells. **D** Representative flow cytometric plots of CD80⁺CD86⁺ DC cells of tumors after treatments. **E** Quantitation of the proportion of mature DCs (CD80⁺CD86⁺) in CD11c⁺ cells. Numerical data are presented as the mean ± SD. *P < 0.05

T (CD45⁺CD8⁺) cells, significant increases were found in the groups of RT combined with nanoparticles compared to other groups (Fig. 5C). Especially in the R837@PLGA@Neu combined with RT group, the percentage of CD8⁺ T cells was even greater than that in the R837@PLGA combined with RT group ($13.70 \pm 2.20\%$ vs. $7.82 \pm 2.58\%$; $P < 0.05$; Fig. 5C). In addition to T cells, the CD11c⁺ cell population was gated to determine the CD80⁺CD86⁺ mature DC (dendritic cell) proportion (Additional file 1: Fig. S4B and Fig. 5D). The percentages of mature DCs were increased to a certain degree in different groups, with the highest percentage in tumors treated with R837@PLGA@Neu combined with RT, which was also significantly higher than that in tumors treated with R837@PLGA combined with RT ($22.56 \pm 4.69\%$ vs. $16.48 \pm 2.76\%$; $P < 0.05$; Fig. 5E). Moreover, macrophages were evaluated by F4/80 and CD206 staining (Additional file 1: Fig. S5A). The percentage of M1 macrophages (F4/80⁺CD206⁻) was highest in the R837@PLGA@Neu combined with RT group (Additional file 1: Fig. S5B), while there were no obvious changes in the percentage of M2 macrophages (F4/80⁺CD206⁺) in the different groups (Additional file 1: Fig. S5C).

R837@PLGA@Neu enhanced the abscopal effect of RT

CT26 cells were inoculated into both flanks of mice to establish bilateral tumor-bearing mice. The mice were treated as shown in Fig. 6A with RT three times only conducted on the right tumor and nanoparticle administration one time via the tail vein. Consistent with Fig. 4, radiated tumors showed prominent tumor inhibition in the RT combined with R837@PLGA@Neu group (Fig. 6B). It was more exciting to find that there was also mild growth inhibition in abscopal tumors without RT with a TGI of 40.29% compared to the control, suggesting the existence of an abscopal effect of RT. However, the abscopal effect of RT was enhanced in the RT combined with R837@PLGA@Neu group with a TGI of 68.13% compared to the RT combined with R837@PLGA group with a TGI of 54.13% (Fig. 6C). Additionally, the tolerance of mice in different groups was good without body weight loss (Fig. 6C). Likewise, RT combined with R837@PLGA@Neu significantly induced cell apoptosis (Fig. 6D, E) and inhibited cell proliferation (Fig. 6F, G) in abscopal xenografts without RT by triggering CD8⁺ T cell infiltration (Fig. 6H and Additional file 1: Fig. S6).

Discussion

As one of the three major treatments for cancer patients, RT is commonly used in combination with chemotherapy in clinical practice to reduce tumor recurrence or metastasis. In recent years, cancer immunotherapy mainly represented by PD-1 or PD-L1 antibodies has become widely known due to its inspiring efficiency in multiple cancers (Marin-Acevedo et al. 2021). Because RT has an immunomodulatory effect on cancer patients, indicated by its abscopal effect, RT combined with immunotherapy has become very popular in various types of cancers and suggests promising synergistic inhibition. It is well known that RT induces DNA damage and promotes the release of tumor-associated antigens (TAAs) (Ngwa et al. 2018) and cytokines (Chen and Mellman 2013), which can activate the immune response of the body.

We know that immune checkpoint inhibitors (ICIs) targeting PD-1 or PD-L1 exert antitumor activity mainly by regulating the T-cell response in the tumor

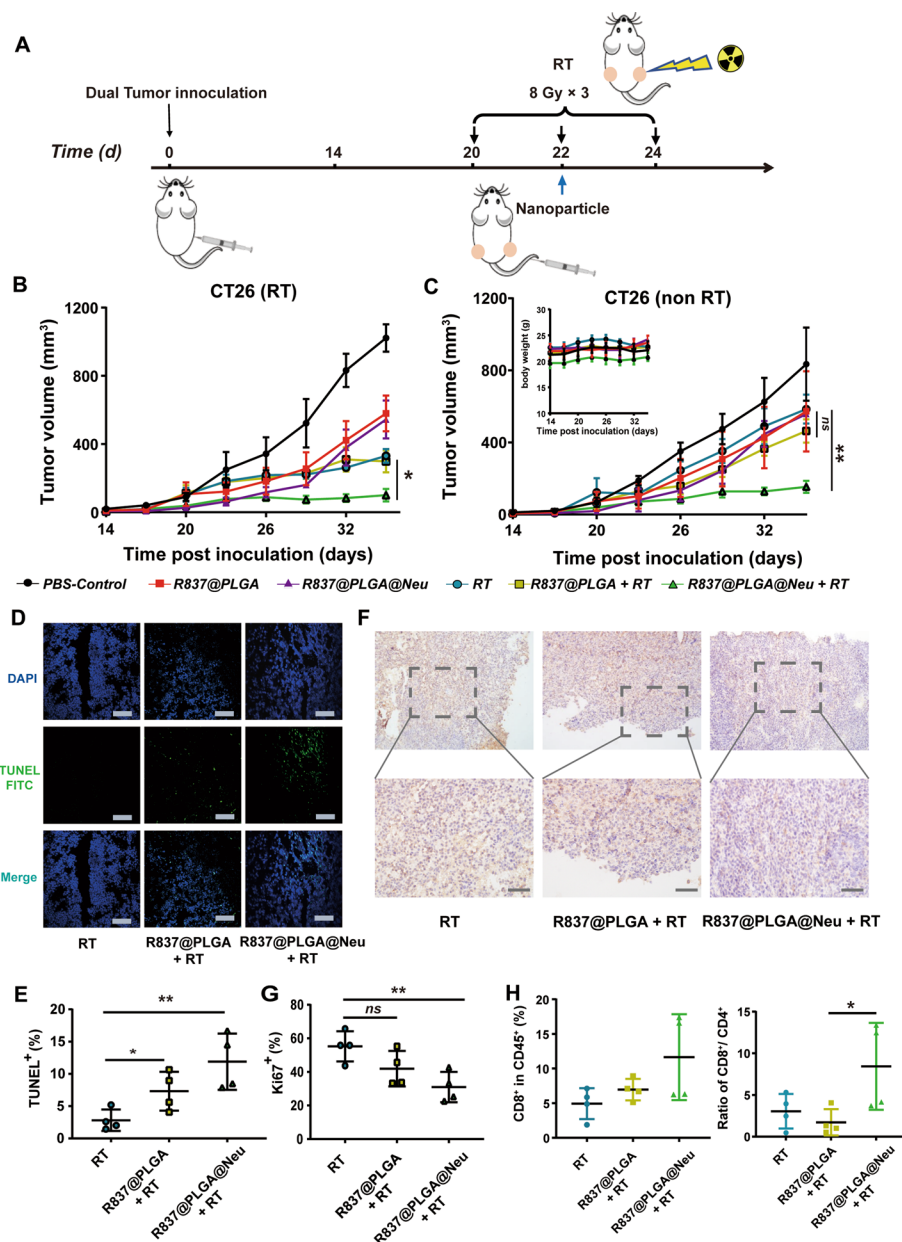


Fig. 6 In vivo abscopal effect of RT combined with R837@PLGA or R837@PLGA@Neu in bilateral CT26 tumor-bearing mice. **A** Schematic illustration of combination therapy in vivo. **B** Tumor growth curves of right irradiated tumors after various treatments. **C** Tumor growth curves of left nonirradiated tumors and body weights of mice after various treatments. **D** Representative images of TUNEL staining in nonirradiated tumor tissues after treatments (scale bar: 50 μm). **E** Quantification of TUNEL-positive cells in tumor sections. **F** IHC staining of Ki67 in nonirradiated tumor tissues after treatments (scale bar: 50 μm). **G** Proportions of Ki67-positive cells in tumor sections. **H** Proportion of CD8⁺ T cells in CD45⁺ cells and ratio of CD8⁺/CD4⁺ cells in nonirradiated tumors by flow cytometry. Numerical data are presented as the mean ± SD. **P* < 0.05; ***P* < 0.01

microenvironment (TME). In addition, activation of the innate immune response also plays an important role in systematic antitumor immunity. Studies have revealed that activation of DCs (dendritic cells) and IFN (interferon) release could enhance RT efficiency via antitumor immunity (Nakajima et al. 2022; Han et al. 2022). Additionally,

agonists of the TLR or cGAS/STING pathway could enhance RT efficacy and induce abscopal effects (Li et al. 2022; Baird et al. 2017). In this study, the TLR7 agonist R837 was used based on our previous study, and R837 was confirmed to induce an antitumor response (Chen et al. 2019; Zhao et al. 2021), as well as its low toxicity in normal cells.

Although R837 displayed antitumor activity, the low water solubility of R837 impedes its use in tumor treatments. To overcome this obstacle, nanoparticle delivery systems have been well investigated. Self-assembled R837 nanoparticles were able to encapsulate R837 to achieve systematic delivery and tumor infiltration (Chen et al. 2019; Zhao et al. 2021). However, the commonly used PLGA delivery system passively accumulated in tumors (Meng et al. 2018), indicating limited tumor permeation of R837 in solid tumors, which was confirmed in our study (Fig. 3D). Therefore, further modifications of nanoparticles are urgently required and will be explored in this study.

Cell membrane coating technology is a frontier approach of biomimetic replication of cell membrane properties, offering an opportunity to combine natural cell membrane properties with those of the artificial inner core material (Liu et al. 2019). Red blood cell membrane coating nanoparticles were identified to have enhanced biocompatibility and tumor targeting (Zhang et al. 2017), suggesting nanoparticles with cell membrane properties. Neutrophils are major immune cells infiltrating tumors to mediate acute inflammation and regulate the immune response (McFarlane et al. 2021). Neutrophils from blood circulation mobilize toward inflammatory site via interactions of CD44 with L-selectin, lymphocyte function-associated antigen-1 with intercellular adhesion molecule-1, and $\beta 1$ integrin with vascular cell adhesion molecule-1 (Kolaczowska and Kubes 2013). Particularly, sustaining release of cytokines in tumors induces persistent recruitment of neutrophils to form neutrophil extracellular traps, which regulates tumor progression (Cristinziano et al. 2022). Recent studies have demonstrated that surgery, RT, or photothermal therapy (PTT) amplified the inflammatory signal of the tumor microenvironment to promote infiltrations of neutrophil (Shen et al. 2021). Various inflammation cytokines in tumors after RT, including TNF- α and IL-8, play an important role in recognition of cell surface integrins for targeting of neutrophils after RT (Barker et al. 2015). In tumors treated with RT, neutrophils are recruited to mediate inflammation and regulate RT sensitivity (Takeshima et al. 2016; Liu et al. 2021). Neutrophils loaded with Abraxane combined with radiotherapy demonstrated high suppression, and vesicles derived from neutrophils showed minimal toxicity and rapid cell uptake (Ju et al. 2019). Based on this, a novel nanoparticle derived from the neutrophil membrane named R837@PLGA@Neu was prepared and investigated in CRC in vitro and in vivo with or without RT. Our novel nanoparticles were identified to have characteristics of low toxicity, high uptake, tumor targeting efficiency, synergistic effect with RT, and enhanced abscopal effect.

Studies have reported that R837 can promote DC maturation, M1/M2 macrophage regulation and CD8⁺ T cell infiltration (Chen et al. 2016; Yang et al. 2018). In our study, R837@PLGA@Neu combined with RT induced a significant increase in CD8⁺ T cells, mature DCs and M1 macrophages, suggesting remodeling of the tumor microenvironment. Moreover, T cells were reported to be one of the most effective

immune cells in inducing the abscopal effect of RT (Ngwa et al. 2018; Formenti et al. 2018), which was consistent with our results that CD8⁺ T cells were increased after treatment with R837@PLGA@Neu combined with RT, indicating a potential systematic immune response in terms of T cell infiltration.

This study suggests the potential prospects of R837@PLGA@Neu nanoparticles in CRC therapy; however, limitations still exist and need to be further investigated. The detailed mechanisms of the accumulation of neutrophil-derived nanoparticles in tumors are unclear. The release of cytokines induced by RT has been considered a major potential mechanism (Citrin et al. 2012; Takeshima et al. 2016). Whether inhibition of cytokines or regression of tumor inflammation inhibited infiltration of neutrophil-derived nanoparticles requires further validation. Recent studies revealed that radiated lesions significantly enhanced infiltration of specific neutrophils related to tumor progression (Nolan et al. 2022). Further research about different types of neutrophils in TME after radiotherapy determines the optimum neutrophils for tumor infiltrations. The release of tumor-associated antigens (TAAs) induced by RT and the antitumor efficiency triggered by TAAs also need to be further investigated. Moreover, the dose and frequency of RT alone or in combination with R837@PLGA@Neu continued to improve due to the complexity and heterogeneity of the tumor and TME. Cell or patient-derived orthotopic xenografts in the colorectum, as well as distant metastatic models, are the optimal choice for preclinical studies (Wang et al. 2019) and should be established to validate the efficacy of R837@PLGA@Neu combined with RT. Additionally, further modification of the PLGA polymer to coalesce multiple drugs to eliminate cancers via multiple mechanisms would be worth exploring in further studies. In brief, there were many scopes that would be pursued based on our novel nanoparticles, which already displayed high translational potential.

Conclusions

In this study, we prepared a novel neutrophil membrane-derived nanoparticle loaded with a TLR7 agonist named R837@PLGA@Neu. Following the identification of its characteristics, we reported that this nanoparticle could augment radiotherapy efficacy and boost abscopal effects by regulating the tumor microenvironment, as indicated by increased mature dendritic cells and CD8⁺ T cells. Our results provide a probable combination strategy for CRC treatment.

Materials and methods

Cell culture and animal models

The murine colon carcinoma cell line CT26 was purchased from American Type Culture Collection (Manassas, VA) and was cultured in RPMI-1640 medium (Invitrogen, Carlsbad, CA) supplemented with 10% fetal bovine serum (FBS) (Gibco, USA) at 37 °C in a humidified atmosphere containing 5% CO₂. Other human CRC cell lines (KM12SM, HT29, HCT116, SW480, SW620) were regularly obtained from our department and cultured in Dulbecco's modified Eagle's medium (DMEM) (Invitrogen, Carlsbad, CA) supplemented with 10% FBS at 37 °C in a humidified atmosphere containing 5% CO₂.

All animal experiments were carried out according to the animal research committee guidelines of Peking University Shenzhen Hospital. Female BALB/c mice (5–6 weeks of

age and 18–20 g body weight) were purchased from GemPharmatech Company (Guangdong, China). For the unilateral tumor-bearing mouse model, a total of 1×10^6 CT26 cells were injected subcutaneously into the right flank of the mouse. For the bilateral tumor-bearing mouse model, 1×10^6 cells were injected subcutaneously into the right and left flanks of mice. Tumor size was measured using a calliper, and tumor volume was calculated as $\text{volume} = \text{length} \times \text{width}^2/2$ (length and width represented the long diameter and short diameter of tumors).

Synthesis of R837@PLGA

PEG-grafted PLGA co-polymer (PEG-PLGA; 50:50 (w/w), Mw ~ 5000:10,000 Da) was purchased from Ruixi Biological Technology Co., Ltd. (Xi'an, China). Synthesis of R837@PLGA and adding doses of nanoparticles were performed according to a previous report (Zhao et al. 2021). Briefly, solid powder of R837 (Aladdin, Shanghai) was dissolved in DMSO at a concentration of 2.5 mg/mL and then added to 10 mg/mL PEG-PLGA dissolved in acetone. The ratio of R837 to PLGA polymer was 1:5 (w/w). In the final water phase, the optimum concentration of R837 was 1.67 mmol/L. The mixture was sonicated at 240 W for 80 s on ice, and then the mixture was dropped into a 5 mL 2.5% w/v solution of polyvinyl alcohol (Sigma-Aldrich, USA). After 1 h of stirring and organic phase evaporation in a rotary evaporator, R837@PLGA nanoparticles were purified after centrifugation at $30,000 \times g$ for 10 min.

Synthesis and characterization of R837@PLGA@Neu

Whole blood from Institute of Cancer Research (ICR) mice collected in heparin tubes was used for the isolation of neutrophils. Blood samples were purified by centrifugation ($400g$, 10 min, 4°C) and then diluted in phosphate buffer solution (PBS) containing ethylene diamine tetraacetic acid (EDTA). The cell pellets were then gently added to the top of a Percoll gradient and centrifuged at $1500 \times g$ for 30 min at room temperature according to the manufacturer's instructions (Solarbio, Beijing). To obtain activated neutrophils, lipopolysaccharide (LPS, 100 ng/mL; Sigma-Aldrich, USA) was added to the culture of neutrophils.

The plasma membrane isolation and nanoparticle-coating process were performed according to previous works (Zhang et al. 2018; Kang et al. 2017). To isolate the plasma membrane from LPS-stimulated neutrophils, the cells were suspended in hypotonic $0.25 \times \text{PBS}$ supplemented with protease inhibitor cocktail, phenylmethanesulfonyl fluoride (PMSF) and EDTA. Then, neutrophils were homogenized for 50 strokes using a Dounce homogenizer with a tight pestle. The homogenate was then centrifuged at $800g$, 4°C , for 10 min to remove the unbroken cells, followed by centrifugation at $10,000g$, 4°C for 30 min to dispose nuclei and the mitochondria by discarding the pellet. The supernatant was centrifuged again at $100,000g$ and 4°C for 1 h. Finally, the cell membrane-containing pellet was washed with PBS containing a protease inhibitor cocktail and EDTA and then freeze-dried, weighed, and stored at -80°C for further use. For the synthesis of R837@PLGA@Neu, the neutrophil membrane (1 mg/mL) was mixed with NPs at a membrane-to-core weight ratio of 1:2, and the mixture was then sonicated at 100 W for 30 s on ice. Nanoparticles derived from neutrophils were prepared as processes including the modest sonication of the mixture for 3 min and the subsequent extrusions using

an Avsetin mini extruder (Avestin, Ottawa) through 400 nm and 200 nm polycarbonate porous membranes 10 times, respectively. DyLight594- or DyLight649-labeled nanoparticles were also prepared in this study.

The morphology and structure of R837@PLGA and R837@PLGA@Neu were characterized using an FEI Tecnai G2 spirit T12 transmission electron microscope (TEMFEI, Hillsboro, USA), and the particle size distribution and zeta potential were measured by dynamic light scattering (Brookhaven Instruments, Holtsville, NY). R837@PLGA or R837@PLGA was dialyzed to detect drug release. Detection of the supernatant by high-performance liquid chromatography (HPLC) with an ultraviolet–visible detector was able to determine the encapsulation efficiency of R837 and the release ratio.

Cytotoxicity and cellular uptake of R837@PLGA@Neu in CRC cells

Logarithmically growing cells were detached from plates using trypsin and plated into 96-well plates at a density of 5×10^3 cells/100 μ L per well. After 24 h, R837@PLGA or R837@PLGA@Neu solutions (0.5 μ mol R837 equivalent/200 μ L in final phase) were added to the cells and cocultured for 24, 48 and 72 h. Finally, 10 μ L of CCK-8 solution (Beyotime, Shanghai) was added to each well and cultured for 2 h at 37 °C. Cell viability based on optical density (OD) at 450 nm was calculated as follows: cell viability = (OD in the intervention wells—blank wells) / (OD in the control wells—blank wells) \times 100%. Three sets of parallel samples not containing nanoparticles served as controls.

CT26 cells were cocultured with DyLight594-labeled R837@PLGA or R837@PLGA@Neu (2.5 mmol/L DyLight549 equivalent concentration) at 37 °C for 24 h and then washed in cold PBS 3 times to remove free nanoparticles. Subsequently, cells were fixed with a mixture of acetone and methanol at a 1:1 ratio for 10 min and stained with phenylindoles (DAPI) for 10 min. Nanoparticle uptake was observed using a fluorescence microscope (Leica, Wetzlar).

Cell uptake was observed in cells under 3D culture conditions. For the generation of 3D spheroids, we used a basement membrane extract (BME)-based method. Briefly, 50 μ L of Matrigel (Corning, NY) was added to a 96-well plate, and a reconstituted basement membrane was formed at 37 °C for 1 h. Then, a cell suspension with a density of 1×10^4 cells/well was seeded on top of the Matrigel. After spheroid formation at Day 4, the spheroids were then used for nanoparticle uptake analysis as described above.

Cell apoptosis detection by Annexin V/PI staining

CT26 cells were seeded onto a 6-well culture plate and treated with R837@PLGA or R837@PLGA@Neu. After 24 h, cells were detached, and cell apoptosis was analyzed with the Annexin V-fluorescein isothiocyanate (FITC)/PI apoptosis detection kit following the manufacturer's instructions (KayGENE Biotech, Nanjing). The samples were analyzed using a CytoFLEX S instrument (Beckman Coulter, California).

In vivo fluorescent imaging of CT26-bearing mice

When xenografts of mice reached approximately 100–200 mm³, mice were injected with DyLight649-labeled R837@PLGA or R837@PLGA@Neu (10 nmol DyLight649 equivalent) in the tail vein. Xenografts were photographed under an IVIS spectrum system (Xenogen, Alameda, CA) at 4, 24 and 48 h postinjection.

In a separate experiment using mice bearing xenografts on both flanks, when the tumor size reached approximately 100–200 mm³, the right tumors in the mice were locally irradiated using an X-ray irradiator (RS2000 PRO, 160 kV, 25 mA; Rad Source Technologies, Suwanee, GA) at a dose rate of 4.12 Gy/min. After the initial 8 Gy of radiation on the right tumors, the mice were intravenously injected with DyLight649-labeled R837@PLGA@Neu. Regions of interest (ROIs) were determined in a living imaging system (Calliper Life Sciences, Hopkinton, USA) for quantitative analysis.

In vivo combination therapy of R837@PLGA@Neu and RT

The mice bearing CT26 tumors with a volume of 50–100 mm³ were divided into the following 6 groups ($n=5-6$ /group): (1) PBS control, (2) R837@PLGA, (3) R837@PLGA@Neu, (4) RT, (5) R837@PLGA + RT, and (6) R837@PLGA@Neu + RT. Mice were injected with R837@PLGA or R837@PLGA@Neu (720 µg of R837 equivalent) via the tail vein. RT was performed 3 times (8 Gy × 3). For each RT session, the tumors were locally irradiated using an X-ray irradiator at a dose rate of 4.12 Gy/min. To study the combination effect of RT and R837@PLGA@Neu, bilateral subcutaneous tumor models were established and randomly divided into 6 groups as previously described in separate experiments. RT was only performed in right tumors 3 times (8 Gy × 3). Tumor size was measured using a calliper, and tumor volume was calculated as $\text{volume} = \text{length} \times \text{width}^2 / 2$ (length and width represented the long diameter and short diameter of tumors).

Treatment efficiency was evaluated by tumor growth inhibition (TGI). TGI was calculated as $\text{TGI} = [1 - (\Delta T / \Delta C)] \times 100\%$ (ΔT and ΔC presented tumor volume changes of treatment group and control group on the last day compared to initial administration, respectively).

Flow cytometric analysis

Xenografts after treatment were digested to obtain single-cell suspensions as previously described (Zhang et al. 2016). The single-cell suspensions of the tumor tissues were suspended in PBS and stained using fluorescently labeled antibodies (Invitrogen, ThermoFisher Scientific, Waltham, MA). For T cell analysis, the single-cell suspensions were stained with FITC-conjugated anti-CD45 (11-0451, clone: 30-F11), allophycocyanin (APC)-conjugated anti-CD4 (17-0042, clone: RM4-5) and phycoerythrin (PE)-conjugated anti-CD8 (12-0081, clone: 53-6.7) antibodies. In the analysis of dendritic cells (DCs), APC-conjugated anti-CD11c (17-0114, clone: N418), FITC-conjugated anti-CD86 (11-0862, clone: GL1) and PE-conjugated anti-CD80 (12-0801, clone: 16-10A1) antibodies were used for staining. FITC-conjugated anti-F4/80 (11-4801, clone: BM8) and PE-conjugated anti-CD206 (12-2061, clone: MR6F3) antibodies were used to stain macrophages. Subsequently, samples were sorted and analyzed using a CytoFLEX S cytometer (Beckman Coulter, California).

Immunohistochemistry staining

For Ki67 staining to quantify cell proliferation, paraffin-embedded tumor tissues after treatments were deparaffinized, the endogenous peroxidase activity was abolished using hydrogen peroxide, and the antigen was retrieved by heated EDTA. Tumor sections 5 µm thick were then incubated with anti-murine Ki67 antibody (ab1667, Clone: SP6, 1:200, Abcam) overnight at 4 °C. Then, sections were incubated with peroxidase-conjugated secondary antibody for 1 h at room temperature and visualized by incubation

with diaminobenzidine substrate (ZSGB-Bio, Beijing). Sections were observed under a microscope (Olympus, Tokyo). The quantification of Ki67-positive cells was determined using ImageJ software (NIH, Bethesda, MD).

TUNEL assay

Frozen tumor sections after treatments were fixed with ice-cold acetone and blocked with 5% bovine serum albumin (BSA) in PBS. TUNEL staining was performed in accordance with the protocols of the Terminal-deoxynucleotidyl Transferase Mediated Nick End Labeling (TUNEL) staining kit (Lablead, Beijing) to detect DNA breakage in apoptotic cells. Briefly, frozen sections were permeated with proteinase K and incubated in equilibration buffer. TUNEL reaction buffer was prepared and added to each sample and reacted at 37 °C for 2 h. The fluorescent signal of YF[®]488 was observed using a fluorescence microscope. The quantification of fluorescence intensity was determined using ImageJ software (NIH, Bethesda, MD).

Statistical analysis

The data obtained for the two groups were analyzed using a two-tailed unpaired Student's *t* test. Comparisons of results before and after treatment were performed using a two-tailed paired Student's *t* test. Comparisons of multiple groups were performed by using one-way analysis of variance (ANOVA) with a post hoc Tukey test. Tumor growth curves were compared by two-way ANOVA. *P* values of <0.05 were considered statistically significant.

Supplementary Information

The online version contains supplementary material available at <https://doi.org/10.1186/s12645-023-00193-8>.

Additional file 1. This file includes: Additional Materials and Methods, **Figures S1 to S6.** **Figure S1.** Characterizations of DyLight594 labeled R837@PLGA@Neu and DyLight649 labeled R837@PLGA@Neu. (A) Hydrodynamic diameters of DyLight594 labeled R837@PLGA. (B) Hydrodynamic diameters of DyLight594 labeled R837@PLGA@Neu. (C) Hydrodynamic diameters of DyLight649 labeled R837@PLGA. (D) Hydrodynamic diameters of DyLight649 labeled R837@PLGA@Neu. **Figure S2.** Tumor growth curve of each mouse bearing unilateral CT26 tumor after various treatments. (A) PBS-control; (B) R837@PLGA; (C) R837@PLGA@Neu; (D) RT; (E) R837@PLGA combined with RT; (F) R837@PLGA@Neu combined with RT. **Figure S3.** H&E staining of organ tissue sections after various treatments. Scale bar: 100 μm. **Figure S4.** Cell gating of flow cytometric analysis of T cells and DCs in CT26 tumors after treatments. (A) Lymphocytes were gated in accordance with cell size. Then T cells were gated in CD45⁺ cell population to analyze CD4⁺ and CD8⁺ T cell proportion. (B) DCs were analyzed in CD11c⁺ cell population, and mature DCs were defined as CD80⁺CD86⁺ cell population. **Figure S5.** Flow cytometric analysis of macrophages in CT26 tumors after treatments. (A) Macrophages were determined by F4/80 staining. F4/80⁺CD206⁻ population was defined as type 1 macrophage (M1), and F4/80⁺CD206⁺ population was defined as type 2 macrophage (M2). (B) Proportion of M1 in tumors after various treatments. (C) Proportion of M2 in tumors after various treatments. Numerical data are presented as mean ± SD. **P* < 0.05. **Figure S6.** Representative flow cytometric plots of CD4⁺ and CD8⁺ T cells in nonirradiated tumors of bilateral tumors bearing mice treated by RT, R837@PLGA combined with RT, and R837@PLGA@Neu combined with RT.

Acknowledgements

This study was supported by the Science, Technology, and Innovation Commission of Shenzhen Municipality (KCXFZ20200201101050887, DSYS20190902092855097, GJHZ20200731095207023), CAS Key Laboratory of Health Informatics, Shenzhen Institute of Advanced Technology (#2011DP173015). A schematic drawing was derived by Figdraw and edited based on export figures (ID: OYTWT6d9d8). HPLC was performed with the assistance of SUSTech Core Research Facilities.

Author contributions

DL conceptualized and wrote the original draft and performed major experiments for data curation and investigation. YX and XY participated in resources and investigation for assistance with small animal investigations. YL, ML and YZ

provided the cell source and technical support. WW provided project administration. YW and SW provided funding acquisition and lab administration. GJ participated in writing, reviewing and editing the manuscript and assisted in data visualization and validation. YL supervised the project and provided funding acquisition. All authors read and approved the final manuscript.

Funding

This study was supported by the Science, Technology, and Innovation Commission of Shenzhen Municipality (KCXFZ20200201101050887, DSYS20190902092855097, GJHZ20200731095207023), CAS Key Laboratory of Health Informatics, Shenzhen Institute of Advanced Technology (#2011DP173015).

Availability of data and materials

The datasets used and/or analyzed during the current study are available from the corresponding author (J.G. and Y. L.) on reasonable request.

Declarations

Ethics approval and consent to participate

All animal experiments were performed by following the protocol approved by the animal research committee guidelines of Peking University Shenzhen Hospital.

Consent for publication

Not applicable.

Competing interests

The authors declare that they have no conflicts of interest.

Received: 20 February 2023 Accepted: 7 April 2023

Published online: 21 April 2023

References

- Baird JR, Monjazeb AM, Shah O, McGee H, Murphy WJ, Crittenden MR et al (2017) Stimulating innate immunity to enhance radiation therapy-induced tumor control. *Int J Radiat Oncol Biol Phys* 99(2):362–373
- Barker HE, Paget JT, Khan AA, Harrington KJ (2015) The tumour microenvironment after radiotherapy: mechanisms of resistance and recurrence. *Nat Rev Cancer* 15(7):409–425
- Cao H, Dan Z, He X, Zhang Z, Yu H, Yin Q et al (2016) Liposomes coated with isolated macrophage membrane can target lung metastasis of breast cancer. *ACS Nano* 10(8):7738–7748
- Chen DS, Mellman I (2013) Oncology meets immunology: the cancer-immunity cycle. *Immunity* 39(1):1–10
- Chen Q, Xu L, Liang C, Wang C, Peng R, Liu Z (2016) Photothermal therapy with immune-adjuvant nanoparticles together with checkpoint blockade for effective cancer immunotherapy. *Nat Commun* 7:13193
- Chen Q, Chen J, Yang Z, Xu J, Xu L, Liang C et al (2019) Nanoparticle-enhanced radiotherapy to trigger robust cancer immunotherapy. *Adv Mater* 31(10):e1802228
- Citrin DE, Hitchcock YJ, Chung EJ, Frandsen J, Urlick ME, Shield W et al (2012) Determination of cytokine protein levels in oral secretions in patients undergoing radiotherapy for head and neck malignancies. *Radiat Oncol* 7:64
- Cristinziano L, Modestino L, Antonelli A, Marone G, Simon HU, Varricchi G et al (2022) Neutrophil extracellular traps in cancer. *Semin Cancer Biol* 79:91–104
- Donlon NE, Power R, Hayes C, Reynolds JV, Lysaght J (2021) Radiotherapy, immunotherapy, and the tumour microenvironment: turning an immunosuppressive milieu into a therapeutic opportunity. *Cancer Lett* 502:84–96
- Formenti SC, Rudqvist NP, Golden E, Cooper B, Wennerberg E, Lhuillier C et al (2018) Radiotherapy induces responses of lung cancer to CTLA-4 blockade. *Nat Med* 24(12):1845–1851
- Gong YK, Winnik FM (2012) Strategies in biomimetic surface engineering of nanoparticles for biomedical applications. *Nanoscale* 4(2):360–368
- Han D, Zhang J, Bao Y, Liu L, Wang P, Qian D (2022) Anlotinib enhances the antitumor immunity of radiotherapy by activating cGAS/STING in non-small cell lung cancer. *Cell Death Discov* 8(1):468
- Hu CM, Zhang L, Aryal S, Cheung C, Fang RH, Zhang L (2011) Erythrocyte membrane-camouflaged polymeric nanoparticles as a biomimetic delivery platform. *Proc Natl Acad Sci U S A* 108(27):10980–10985
- Ito H (2016) Combination therapy with TLR7 agonist and radiation is effective for the treatment of solid cancer. *Ann Transl Med* 4(5):95
- Ju C, Wen Y, Zhang L, Wang Q, Xue L, Shen J et al (2019) Neoadjuvant chemotherapy based on abraxane/human neutrophils cytopharmaceuticals with radiotherapy for gastric cancer. *Small* 15(5):e1804191
- Kang T, Zhu Q, Wei D, Feng J, Yao J, Jiang T et al (2017) Nanoparticles coated with neutrophil membranes can effectively treat cancer metastasis. *ACS Nano* 11(2):1397–1411
- Kolaczowska E, Kubes P (2013) Neutrophil recruitment and function in health and inflammation. *Nat Rev Immunol* 13(3):159–175
- Li J, Ren H, Qiu Q, Yang X, Zhang J, Zhang C et al (2022) Manganese coordination micelles that activate stimulator of interferon genes and capture in situ tumor antigens for cancer metalloimmunotherapy. *ACS Nano* 16(10):16909–16923
- Liu Y, Luo J, Chen X, Liu W, Chen T (2019) Cell membrane coating technology: a promising strategy for biomedical applications. *Nanomicro Lett* 11(1):100
- Liu Q, Hao Y, Du R, Hu D, Xie J, Zhang J et al (2021) Radiotherapy programs neutrophils to an antitumor phenotype by inducing mesenchymal-epithelial transition. *Transl Lung Cancer Res* 10(3):1424–1443

- Marin-Acevedo JA, Kimbrough EO, Lou Y (2021) Next generation of immune checkpoint inhibitors and beyond. *J Hematol Oncol* 14(1):45
- McFarlane AJ, Fercoq F, Coffelt SB, Carlin LM (2021) Neutrophil dynamics in the tumor microenvironment. *J Clin Invest* 131:6
- Meng L, Cheng Y, Tong X, Gan S, Ding Y, Zhang Y et al (2018) Tumor oxygenation and hypoxia inducible factor-1 functional inhibition via a reactive oxygen species responsive nanoplatfor for enhancing radiation therapy and abscopal effects. *ACS Nano* 12(8):8308–8322
- Miller RL, Gerster JF, Owens ML, Slade HB, Tomai MA (1999) Imiquimod applied topically: a novel immune response modifier and new class of drug. *Int J Immunopharmacol* 21(1):1–14
- Miller KD, Nogueira L, Mariotto AB, Rowland JH, Yabroff KR, Alfano CM et al (2019) Cancer treatment and survivorship statistics, 2019. *CA Cancer J Clin* 69(5):363–385
- Nakajima S, Mimura K, Kaneta A, Saito K, Katagata M, Okayama H et al (2022) Radiation-induced remodeling of the tumor microenvironment through tumor cell-intrinsic expression of cGAS-STING in esophageal squamous cell carcinoma. *Int J Radiat Oncol Biol Phys* 78:5
- Ngwa W, Irabor OC, Schoenfeld JD, Hesser J, Demaria S, Formenti SC (2018) Using immunotherapy to boost the abscopal effect. *Nat Rev Cancer* 18(5):313–322
- Nolan E, Bridgeman VL, Ombrato L, Karoutas A, Rabas N, Sewnath CAN et al (2022) Radiation exposure elicits a neutrophil-driven response in healthy lung tissue that enhances metastatic colonization. *Nat Cancer* 3(2):173–187
- Panelli MC, Stashower ME, Slade HB, Smith K, Norwood C, Abati A et al (2007) Sequential gene profiling of basal cell carcinomas treated with imiquimod in a placebo-controlled study defines the requirements for tissue rejection. *Genome Biol* 8(1):R8
- Reynders K, Illidge T, Siva S, Chang JY, De Ruyscher D (2015) The abscopal effect of local radiotherapy: using immunotherapy to make a rare event clinically relevant. *Cancer Treat Rev* 41(6):503–510
- Shen J, Hao J, Chen Y, Liu H, Wu J, Hu B et al (2021) Neutrophil-mediated clinical nanodrug for treatment of residual tumor after focused ultrasound ablation. *J Nanobiotechnol* 19(1):345
- Takeshima T, Pop LM, Laine A, Iyengar P, Vitetta ES, Hannan R (2016) Key role for neutrophils in radiation-induced antitumor immune responses: potentiation with G-CSF. *Proc Natl Acad Sci U S A* 113(40):11300–11305
- Varshney D, Qiu SY, Graf TP, McHugh KJ (2021) Employing drug delivery strategies to overcome challenges using TLR7/8 agonists for cancer immunotherapy. *AAPS J* 23(4):90
- Walshaw RC, Honeychurch J, Choudhury A, Illidge TM (2020) Toll-like receptor agonists and radiation therapy combinations: an untapped opportunity to induce anticancer immunity and improve tumor control. *Int J Radiat Oncol Biol Phys* 108(1):27–37
- Wang J, Xing B, Liu W, Li J, Wang X, Li J et al (2019) Molecularly annotation of mouse avatar models derived from patients with colorectal cancer liver metastasis. *Theranostics* 9(12):3485–3500
- Xu L, Zou C, Zhang S, Chu TSM, Zhang Y, Chen W et al (2022) Reshaping the systemic tumor immune environment (STIE) and tumor immune microenvironment (TIME) to enhance immunotherapy efficacy in solid tumors. *J Hematol Oncol* 15(1):87
- Yang R, Xu J, Xu L, Sun X, Chen Q, Zhao Y et al (2018) Cancer cell membrane-coated adjuvant nanoparticles with mannose modification for effective anticancer vaccination. *ACS Nano* 12(6):5121–5129
- Zhang C, Gao L, Cai Y, Liu H, Gao D, Lai J et al (2016) Inhibition of tumor growth and metastasis by photoimmunotherapy targeting tumor-associated macrophage in a sorafenib-resistant tumor model. *Biomaterials* 84:1–12
- Zhang Y, Zhang J, Chen W, Angsantikul P, Spiekermann KA, Fang RH et al (2017) Erythrocyte membrane-coated nanogel for combinatorial antivirulence and responsive antimicrobial delivery against *Staphylococcus aureus* infection. *J Control Release* 263:185–191
- Zhang Y, Cai K, Li C, Guo Q, Chen Q, He X et al (2018) Macrophage-membrane-coated nanoparticles for tumor-targeted chemotherapy. *Nano Lett* 18(3):1908–1915
- Zhao Y, Zhang T, Wang Y, Lu D, Du J, Feng X et al (2021) ICAM-1 orchestrates the abscopal effect of tumor radiotherapy. *Proc Natl Acad Sci U S A* 118(14):e2010333118

Publisher's Note

Springer Nature remains neutral with regard to jurisdictional claims in published maps and institutional affiliations.

Ready to submit your research? Choose BMC and benefit from:

- fast, convenient online submission
- thorough peer review by experienced researchers in your field
- rapid publication on acceptance
- support for research data, including large and complex data types
- gold Open Access which fosters wider collaboration and increased citations
- maximum visibility for your research: over 100M website views per year

At BMC, research is always in progress.

Learn more biomedcentral.com/submissions

